Research Article Vol. 6, No. 3 / March 2019 / Optica 335

optica

Scalable feedback control of single photon sources for photonic quantum technologies

JACQUES CAROLAN,[1,*] UTTARA CHAKRABORTY,[1] NICHOLAS C. HARRIS,[2] MIHIR PANT,[1] TOM BAEHR-JONES,[3] MICHAEL HOCHBERG,[3] AND DIRK ENGLUND[1]

[1]Research Laboratory of Electronics, Massachusetts Institute of Technology, Cambridge, Massachusetts 02139, USA
[2]Lightmatter, 61 Chatham St 5th floor, Boston, Massachusetts 02109, USA
[3]Elenion Technologies, 171 Madison Avenue, Suite 1100, New York, New York 10016, USA
*Corresponding author: carolanj@mit.edu

Received 13 December 2018; revised 12 February 2019; accepted 12 February 2019 (Doc. ID 355233); published 8 March 2019

Large-scale quantum technologies require exquisite control over many individual quantum systems. Typically, such systems are very sensitive to environmental fluctuations, and diagnosing errors via measurements causes unavoidable perturbations. In this work, we present an *in situ* frequency-locking technique that monitors and corrects frequency variations in single photon sources based on microring resonators. By using the same classical laser fields required for photon generation as probes to diagnose variations in the resonator frequency, our protocol applies feedback control to correct photon frequency errors in parallel to the optical quantum computation without disturbing the physical qubit. We implement our technique on a silicon photonic device and demonstrate sub 1 pm frequency stabilization in the presence of applied environmental noise, corresponding to a fractional frequency drift of <1% of a photon linewidth. Using these methods, we demonstrate feedback-controlled quantum state engineering. By distributing a single local oscillator across a single chip or network of chips, our approach enables frequency locking of many single photon sources for large-scale photonic quantum technologies.

https://doi.org/10.1364/OPTICA.6.000335

1. INTRODUCTION

Precise and robust control over individual quantum systems is a prerequisite for any scalable quantum technology. In photonic quantum technologies [1,2], single photons are generated via a nonlinear optical process [3,4], propagated through linear optical circuitry [5,6], and read out via single photon detectors [7]. Each of these core components has been demonstrated within the silicon (Si) photonics platform [8] providing a plausible route towards millions of quantum optical components within a single wafer [9,10]. As systems scale up [11,12], techniques for error mitigation in quantum optical devices have become paramount. Tools have been developed for pre-characterization of circuitry via classical laser fields [13,14], but until now, techniques for actively monitoring errors have been outstanding.

In this work, we introduce a new *in situ* control technique for photonic quantum technologies [shown in Fig. 1(a)] that tracks and corrects variations in single photon sources based on microring resonators (MRRs), without the need for destructive quantum measurements. Microring resonators [15] are a leading approach to the generation of ultra-bright [4,14] and pure [16] single photons via the process of spontaneous four-wave mixing, with the resonance structure enabling directly engineered photon frequencies in a tens of micrometer-scale footprint. In the degenerate case where the generated photons are the same wavelength [see Fig. 1(b)], the MRR is pumped by two lasers tuned to $\omega_{p_1}, \omega_{p_2}$, corresponding to the $+n$th and $-n$th resonances of the ring. A photon at each frequency is spontaneously annihilated within the resonator to generate two correlated signal and idler photons at the frequency $\omega_{s,i} = (\omega_{p_1} + \omega_{p_2})/2$ in the $n = 0$th resonance of the ring, conserving energy.

Our protocol makes use of a unique property of photonic quantum technologies where much of the error diagnosis and correction can be implemented via classical laser fields at high bandwidth, and with an intrinsically high signal-to-noise ratio. Using the same laser fields that seed photon generation as local oscillators to diagnose cavity fluctuations, we develop a closed-loop protocol that corrects single photon frequency errors. We implement a proof-of-concept demonstration of our technique on a Si quantum photonic device, and, by stabilizing on-chip cavities to sub 1 pm levels at the DC limit (corresponding to a fractional frequency drift of <1% a cavity linewidth), correct static errors between photon sources, track and correct dynamic errors, and demonstrate feedback-controlled quantum state engineering. Our corrections are performed in parallel to quantum information processing and can be scaled to many thousands of optical components.

In large-scale architectures such as those required for quantum advantage [17,18], quantum simulation [19–21], or quantum computing [22], many MRRs must be tuned to precisely the same frequency. Misalignment between resonators reduces quantum interference, which can cause errors on the photonic qubit [23,24]. Moreover, the efficiency and brightness of such sources scale cubicly with the quality factor of the resonator [25], placing stringent demands on the stability of MRR structures. Fabrication variations will cause *static errors* in the resonance of the MRRs, while variations in refractive index over time—due to thermal fluctuations, introduction of carriers, electrical noise, or crosstalk between devices—will introduce *dynamic errors*.

Device-level feedback control techniques typically measure the qubit, estimate some fidelity metric, and feed back onto the control parameters to minimize the infidelity in a closed-loop manner [26,27]. The success of these so-called *in situ* control techniques hinges upon the efficiency and robustness of the fidelity estimator [28]. Our approach shown in Fig. 1(c) monitors the pump frequency modes with a low-loss drop filter and photodiode. If the central frequency of the resonator shifts, the optical power on the photodiode increases, and an electrical signal is fed back onto the phase shifter in a closed-loop manner to decrease the optical power. This minimization can be implemented in either software (e.g., computational optimization) or hardware (e.g., lock-in amplifier [29]). Our closed-loop protocol scales with a time complexity $\mathcal{O}(1)$ in the number of MRRs, and is typically bandwidth limited by the control phase modulator. Each constituent component has already been demonstrated in standard CMOS Si photonic processes: low-loss filtering [30], fast photodiodes [31], and phase modulation [including thermo-optic (kHz [32]), microelectromechanical (MHz [33]) and carrier-based (GHz [34])]. Moreover, the classical probe signal provides an intrinsically high signal-to-noise ratio compared with direct detection of the photons.

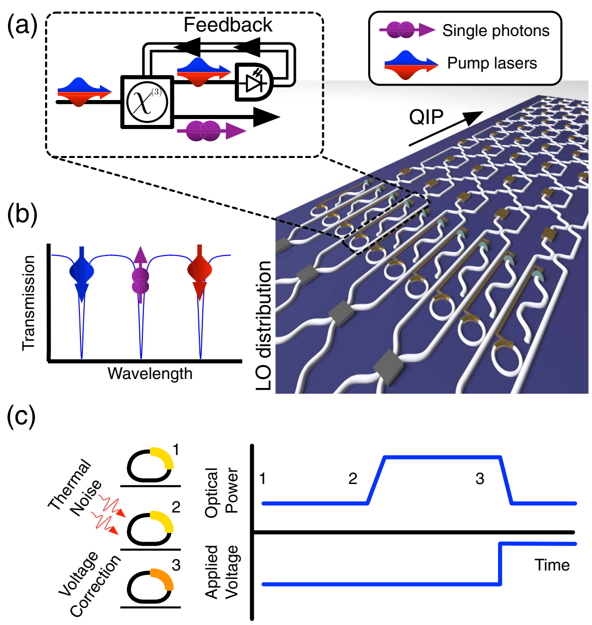

Fig. 1. Proposed architecture for *in situ* photon source stabilization. (a) A pump field is coupled into a Kerr-based resonator structure, which produces correlated photons via spontaneous four-wave mixing. The pump field is monitored via a photodiode, which is fed back onto the resonator to stabilize the central frequency. By distributing a single pump (local oscillator, LO) across an entire chip, many thousands of resonators can be frequency locked in parallel to enable large-scale quantum information processing (QIP). (b) Transmission spectrum of a single microring resonator. Pump lasers are tuned to the $i-1$th and $i+1$th resonance of the ring to generate two single photons at the ith resonance. (c) The photodiode measures an initial optical power (1); if the resonance of the MRR shifts due to, say, thermal fluctuations, the power in the pump modes increases (2), which is then corrected via a closed-loop feedback on the ring phase shifter (3).

2. DEVICE

For our proof-of-concept demonstration, we use a quantum state engineering Si photonic device, alongside off-chip pump separation and monitoring. The device produces correlated pairs of photons via the inverse Hong–Ou–Mandel effect [3] and comprises five stages, as shown in Fig. 2(a). The first mixes the two pumps on a 50/50 directional coupler. Next, the mixed pumps impinge on a photon generation MRR in each arm of a Mach–Zehnder interferometer. The pump power is partially reduced via demux filters to prevent further photon generation in the waveguides, yet remains at a level sufficient to be monitored via off-chip photodiodes. The state passes through a differential phase ϕ, and by operating in the weak pumping regime such that an appreciable probability exists of producing only two photons, the quantum state after the two rings is $|\psi\rangle_{\text{ring}} = (|20\rangle_{1,2} + e^{2i\phi}|02\rangle_{1,2})/\sqrt{2}$, where $|n\rangle_m$ represents n photons in the mth optical mode. Finally, the state is incident on a 50/50 directional coupler, which yields the state

$$|\psi(\phi)\rangle_{\text{out}} = \cos\phi(|20\rangle - |02\rangle)/\sqrt{2} + \sin\phi|11\rangle. \quad (1)$$

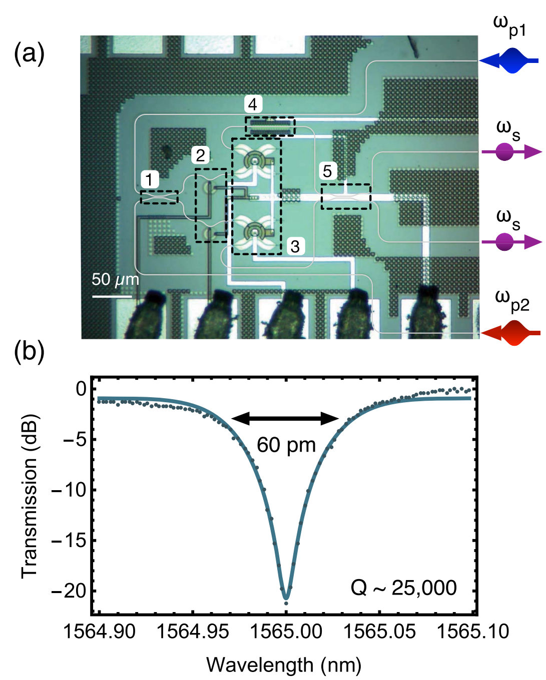

Fig. 2. Quantum state engineering photonic device. (a) Optical micrograph of the silicon photonic device that incorporates five thermo-optically controlled phases shifters and four microring resonators (two for photon generation and two for pump suppression) in just 0.08 mm^2. Marked components represent the five stages required for quantum state engineering: (1) pump mixing on a directional coupler, (2) photon generation in two MRRs, (3) partial pump suppression in two further MRRs, (4) differential phase shift, and (5) final directional coupler for quantum interference. (b) Optical spectrograph of the two generation rings aligned to 1565 nm alongside expected fit.

Control of the differential phase therefore enables state engineering, including tuning between path entangled states ($\phi = 0$) and separable states ($\phi = \pi$).

The chip, fabricated in a standard CMOS Si photonics process, contains four MRRs and five thermo-optic phase shifters, all within 0.08 mm^2 [see Fig. 2(a)]. The spectrum of the photon generation MRR is shown in Fig. 2(b). Each ring has with a linewidth $\Delta\lambda = 60$ pm, yielding a quality factor of $Q \approx 2.5 \times 10^4$. Light is in/out-coupled via a custom-built silicon nitride optical interposer, which matches both the mode field diameter and pitch of the Si waveguides to give a loss of -2.5 ± 0.5 dB per facet (error determined by multiple measurements). At the input, two tunable telecommunication lasers are pre-filtered to reduce optical sidebands at the photon generation wavelength. At the output, photons are first filtered to enable pump monitoring and reduce background, then coupled into superconducting nanowire single photon detectors with ~75% quantum efficiency. See Supplement 1 for further experimental details.

3. PROTOCOL

As a first test of our frequency-locking protocol, we correct static errors in the resonance position of the generation rings, which can occur due to fabrication variations such as waveguide surface roughness [35]. In principle, accurate characterization of wavelength-voltage tuning curves can correct for this effect, but as we show, noise sources such as thermal crosstalk and electrical noise complicate this process, necessitating an *in situ* approach. For this test, the feedback correction protocol is run 100 times. Each run sets the pump laser to the desired generation wavelength, and initial voltages for the two generation rings are chosen randomly from normal distributions centered on 3.60 V

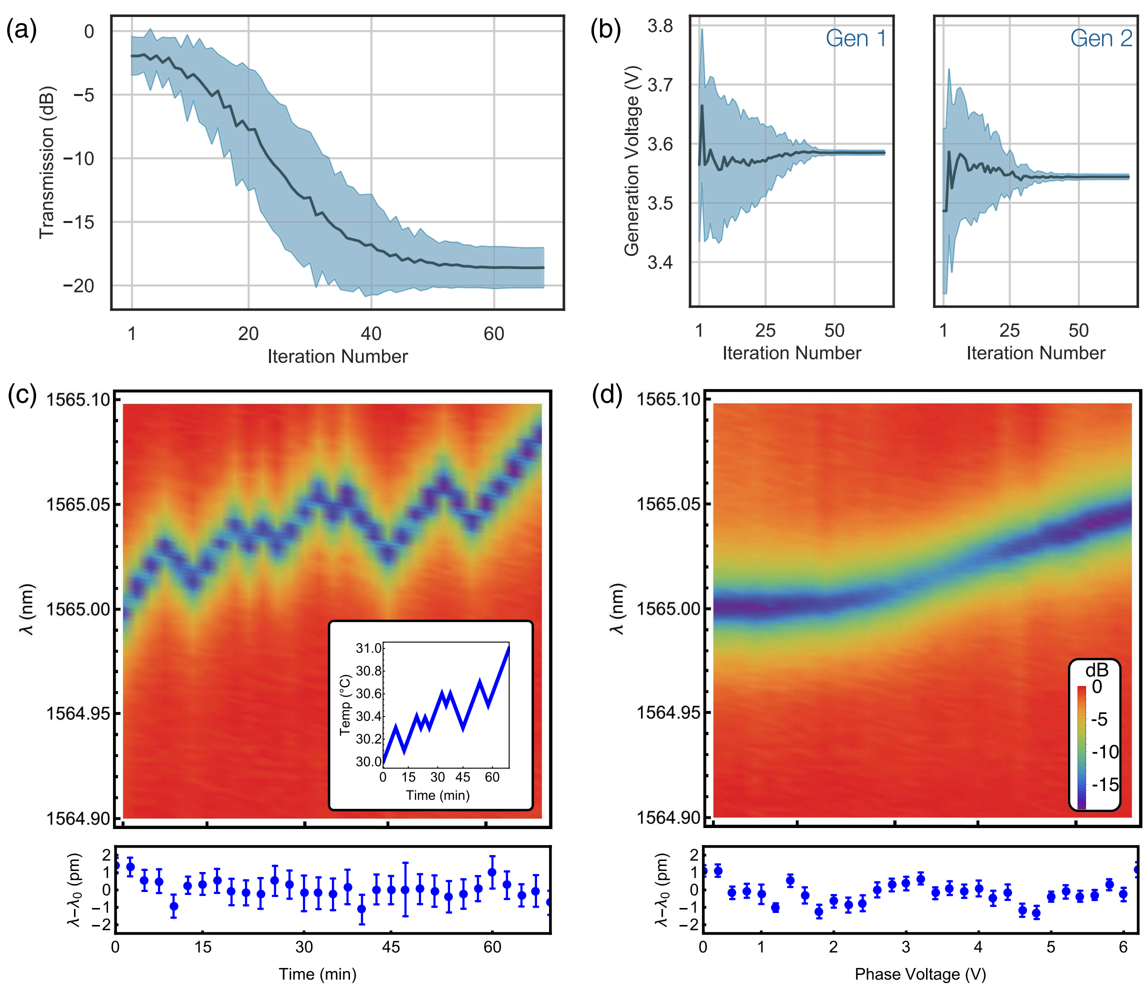

Fig. 3. Static and dynamic feedback correction. (a) Mean of 62 instances of static frequency feedback correction, with initial guess voltages for each run randomly and independently chosen (see text). The shaded region represents $\pm 1\sigma$. With the pump laser set to the desired alignment frequency of $\lambda_0 = 1565$ nm, the voltage on each generation MRR is optimized to minimize the sum of the optical power in two output modes. (b) Mean change in voltages for each generation MRR during all 62 alignment protocols. Solution voltages vary not only between MRRs (a static offset due to fabrication variations) but also over the course of the experiment due to a systematic change in laboratory conditions. (c) Spectrograph of the MRRs as a function of applied thermal noise (inset) over the course of 1 h in the absence of dynamic stabilization. Spectrographs are taken by tuning an auxiliary laser and measuring the output power on a photodiode. Given the same applied noise model, the bottom plot shows the variation in central resonance when dynamic frequency stabilization is applied. Error bars are given by the error in the resonance fit. (d) Spectrograph of the MRRs as a voltage is applied to an adjacent thermo-optic phase shifter. Thermal crosstalk causes the resonance of the MRRs to shift, which should otherwise remain untouched by the phase shifter. The bottom plot shows the variation when dynamic frequency stabilization is applied. In each instance, the dynamic stabilization gives a two orders of magnitude increase in the resonance stability.

and 3.56 V (independently determined to be near optimal), respectively, with a standard deviation of 0.2 V. Computational optimization is used to iteratively arrive at the generation ring voltage combination that minimizes the sum of the optical output powers of the MRRs as measured by an off-chip photodiode array. In Supplement 1, we provide a mathematical model for this system. The Nelder–Mead algorithm [36] was empirically determined to converge quickly and be robust in the presence of experimental noise. This numerical technique operates on both phase shifters simultaneously to determine the optimum in a derivative-free manner. As shown in Fig. 3(a), out of the 100 attempted runs, 62 succeed, requiring an average of 57 iterations to converge. Figure 3(b) tracks the voltages of each generation MRR during optimization. The final voltage of each ring differs by 40 mV, demonstrating the importance of static error correction. Moreover, repeatedly running this protocol over the course of 7 h, we observe a total reduction in the voltages by 18 mV, likely due to a systematic drift in laboratory temperature.

In Figs. 3(c) and 3(d), we simulate two classes of dynamic error typically seen in photonic quantum systems: (1) environmental temperature fluctuations and (2) crosstalk between thermo-optic phase shifters. We induce temperature fluctuations by varying the chip temperature through an auxiliary Peltier control system onto which the device is mounted. In increments and decrements of 0.1°C, we program a random walk in temperature over the course of 1 h for a net increase of 1°C. One instance of this random walk is shown in the Fig. 3(c) inset. Figure 3(c) plots spectrographs for this instance that show the shift in central resonance of the MRRs as a result of this temperature variation in the absence of dynamic frequency stabilization and in the presence of our *in situ* approach. The implementation of our protocol leads to a standard deviation in the central resonance wavelength of 0.56 pm ($9.4 \times 10^{-3}\Delta\lambda$), compared to a total variation of 84.0 pm ($1.4\Delta\lambda$) in the absence of any correction protocol. This corresponds to a two-orders of magnitude increase in resonance stability.

Similarly, we induce thermal crosstalk by sweeping the phase-shifter voltage from 0 V to 6.5 V. Figure 3 shows the central wavelength shift in (c) the uncorrected case, and (d) the *in situ* corrected case. Dynamic frequency stabilization yields a stability of 0.65 pm ($1.1 \times 10^{-2}\Delta\lambda$), a 70-fold improvement compared with a total variation of 45 pm ($0.75\Delta\lambda$) in the uncorrected case.

We contrast the performance of our *in situ* correction technique with the results obtained using pre-determined tuning curve models (see Supplement 1 for details) to align the rings, with the same temperature or phase-shifter voltage adjustment. After each adjustment, the generation ring voltages are set to the values according to pre-determined functions. While alignment using pre-determined functions leads to a 15-fold and 5-fold improvement over the uncorrected case for the temperature and voltage error, respectively, our iterative protocol still outperforms the tuning-curve-based correction by an order of magnitude in both instances. Moreover, our technique can naturally be applied to dynamic corrections where no noise model is known.

The merit of the *in situ* approach is that it can be performed in parallel to quantum computation. To demonstrate this, our protocol is applied to the task of quantum state engineering. According to Eq. (1), a linear variation in the differential phase ϕ causes a sinusoidal change in the probability amplitude of the $|11\rangle$ state, and a sine-squared change in the coincidence probability. Control of the thermo-optic phase shifter thus provides a direct means to engineer the photonic quantum state. In the absence of frequency control [Fig. 4(a), red] thermal crosstalk from the differential phase decouples the MRRs and causes an asymmetry in the interference fringe. To quantify this effect, we introduce the asymmetric contrast $C_{\text{asy}} = |C_1 - C_2|/\max(C_1, C_2)$, which is the normalized difference between the coincidence counts C_1 at $\phi = \pi/2$ and counts C_2 at $\phi = 3\pi/2$, where $C_{\text{asy}} = 0$ in the ideal case. In the absence of correction, $C_{\text{asy}} = 0.791$.

The frequency control protocol is implemented at each step of the phase sweep [Fig. 4(a), blue], correcting the generation voltages [Fig. 4(b)] and recovering the symmetry of the interference fringe, yielding a contrast $C_{\text{asy}} = 5.61 \times 10^{-3}$. The quantum visibility quantifies the indistinguishability of the photons and is given by $V_q = (C_{\max} - C_{\min})/C_{\max}$, where $C_{\max}(C_{\min})$ is the maximum (minimum) measured coincidence counts. The interference fringe is fitted [Fig. 4(a), blue line] to account for the nonlinear phase-voltage relation of the thermo-optic phase shifter [32], and the quantum visibility is extracted as $V_q = 0.938 \pm 0.021$. The deviation from unity visibility is due primarily to higher-order

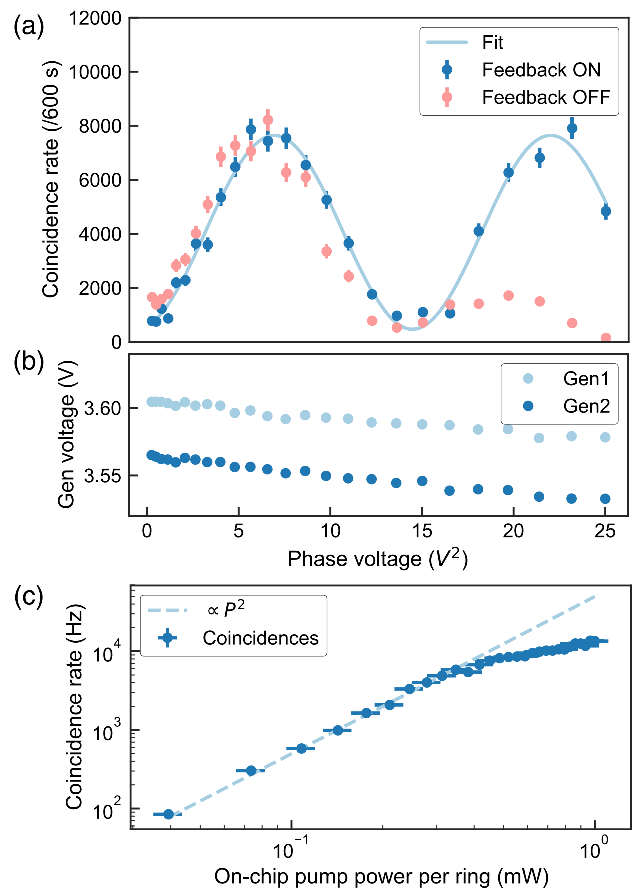

Fig. 4. Quantum state engineering. (a) Coincidence count rate plotted as a function of the square of the differential phase voltage, with (blue) and without (red) frequency stabilization, alongside a sinusoidal fit (light blue). Coincidences have been normalized for detector channel inefficiencies, and error bars assume Poissonian counting statistics. The symmetry in the locked fringe can clearly be observed in comparison to the unlocked. (b) Variation in MRR control voltages over the course of the differential phase sweep when frequency locking is applied. (c) Coincidence count rate plotted as a function of input power per ring (blue points) and an expected quadratic dependency based on a purely four-wave mixing process (light blue line).

photon events, which occur due to the high pump power required to obtain a reasonable signal-to-noise ratio in the presence of lossy off-chip filters. In the future, the monolithic integration of lasers [37], single photon detectors [7], and filters [4,38] will significantly reduce optical power constraints.

Finally, in Fig. 4(c), with $\phi = \pi/2$, we measure the coincidence count rate as a function of the input pump power. At each optical power setting, we apply the frequency stabilization protocol to account for the refractive index change in the MRRs due to a combination of Kerr, thermal, and free-carrier dispersion effects [39]. We reach an off-chip photon generation rate of 13.5 kHz (corrected for detector channel inefficiencies), which is limited primarily by two-photon absorption. This can be seen in Fig. 4(c), where we plot the measured coincidence count rate against the expected quadratic dependence [Fig. 4(c), blue dashed], observing deviations at powers greater than 200 μW. Significant progress is being made on mid-IR silicon photonics that will mitigate the effect of two-photon absorption, which becomes negligible at wavelengths longer than 2.2 μm [40,41].

4. CONCLUSION

We have proposed and demonstrated an *in situ* control technique for photonic quantum technologies that uses the same classical laser fields required for photon generation as a probe to track, diagnose, and correct frequency variations in single photon sources. While feedback control in our device is applied off-chip, *in situ* feedback was recently demonstrated in an integrated CMOS photonics platform [10]. Electronic control circuitry integrated either on-chip [42] or via flip-chip approaches [43], would therefore allow large numbers of heralded single photon sources to be frequency locked to a common local oscillator. The combination of Kerr nonlinear optics in silicon rings with CMOS logic and single photon detection [7,44–46] could enable on-demand high-fidelity single photon sources based on multiplexed spontaneous four-wave mixing [47], which form the basis of the proposed all-optical quantum computing [9] and quantum repeater architectures [48].

Funding. Air Force Office of Scientific Research (AFOSR) (FA9550-14-1-0052, FA9550-16-1-0391); H2020 Marie Skłodowska-Curie Actions (MSCA) (751016); National Defense Science and Engineering Graduate Fellowship.

Acknowledgment. We gratefully acknowledge A. Pyke, at Aerospace Semiconductor, as well as C. Panuski, C. Chen, F. Wong, and J. Combes. J. C. is supported by MSCA. U. C. is supported by the National Defense Science and Engineering Graduate Fellowship.

See Supplement 1 for supporting content.

REFERENCES

1. J. L. O'Brien, "Optical quantum computing," Science **318**, 1567–1570 (2007).
2. J. L. O'Brien, A. Furusawa, and J. Vučković, "Photonic quantum technologies," Nat. Photonics **3**, 687–695 (2009).
3. J. W. Silverstone, D. Bonneau, K. Ohira, N. Suzuki, H. Yoshida, N. Iizuka, M. Ezaki, C. M. Natarajan, M. G. Tanner, R. H. Hadfield, V. Zwiller, G. D. Marshall, J. G. Rarity, J. L. O'Brien, and M. G. Thompson, "On-chip quantum interference between silicon photon-pair sources," Nat. Photonics **8**, 104–108 (2014).
4. N. C. Harris, D. Grassani, A. Simbula, M. Pant, M. Galli, T. Baehr-Jones, M. Hochberg, D. Englund, D. Bajoni, and C. Galland, "Integrated source of spectrally filtered correlated photons for large-scale quantum photonic systems," Phys. Rev. X **4**, 041047 (2014).
5. J. Carolan, C. Harrold, C. Sparrow, E. Martn López, N. J. Russell, J. W. Silverstone, P. J. Shadbolt, N. Matsuda, M. Oguma, M. Itoh, G. D. Marshall, M. G. Thompson, J. C. F. Matthews, T. Hashimoto, J. L. O'Brien, and A. Laing, "Universal linear optics," Science **349**, 711–716 (2015).
6. N. C. Harris, J. Carolan, D. Bunandar, M. Prabhu, M. Hochberg, T. Baehr-Jones, M. L. Fanto, A. M. Smith, C. C. Tison, P. M. Alsing, and D. Englund, "Linear programmable nanophotonic processors," Optica **5**, 1623–1631 (2018).
7. F. Najafi, J. Mower, N. C. Harris, F. Bellei, A. Dane, C. Lee, X. Hu, P. Kharel, F. Marsili, S. Assefa, K. K. Berggren, and D. Englund, "On-chip detection of non-classical light by scalable integration of single-photon detectors," Nat. Commun. **6**, 5873 (2015).
8. J. W. Silverstone, D. Bonneau, J. L. O'Brien, and M. G. Thompson, "Silicon quantum photonics," IEEE J. Sel. Top. Quantum Electron. **22**, 390–402 (2016).
9. T. Rudolph, "Why I am optimistic about the silicon-photonic route to quantum computing," APL Photon. **2**, 030901 (2017).
10. C. Sun, M. T. Wade, Y. Lee, J. S. Orcutt, L. Alloatti, M. S. Georgas, A. S. Waterman, J. M. Shainline, R. R. Avizienis, S. Lin, B. R. Moss, R. Kumar, F. Pavanello, A. H. Atabaki, H. M. Cook, A. J. Ou, J. C. Leu, Y.-H. Chen, K. Asanović, R. J. Ram, M. A. Popović, and V. M. Stojanović, "Single-chip microprocessor that communicates directly using light," Nature **528**, 534–538 (2015).
11. N. C. Harris, G. R. Steinbrecher, M. Prabhu, Y. Lahini, J. Mower, D. Bunandar, C. Chen, F. N. C. Wong, T. Baehr-Jones, M. Hochberg, S. Lloyd, and D. Englund, "Quantum transport simulations in a programmable nanophotonic processor," Nat. Photonics **11**, 447–452 (2017).
12. J. Wang, S. Paesani, Y. Ding, R. Santagati, P. Skrzypczyk, A. Salavrakos, J. Tura, R. Augusiak, L. Mančinska, D. Bacco, D. Bonneau, J. W. Silverstone, Q. Gong, A. Acn, K. Rottwitt, and L. K. Oxenløwe, J. L. O'Brien, A. Laing, and M. G. Thompson, "Multidimensional quantum entanglement with large-scale integrated optics," Science **360**, 285–291 (2018).
13. S. Rahimi-Keshari, M. A. Broome, R. Fickler, A. Fedrizzi, T. C. Ralph, and A. G. White, "Direct characterization of linear-optical networks," Opt. Express **21**, 13450–13459 (2013).
14. D. Grassani, A. Simbula, S. Pirotta, M. Galli, M. Menotti, N. C. Harris, T. Baehr-Jones, M. Hochberg, C. Galland, M. Liscidini, and D. Bajoni, "Energy correlations of photon pairs generated by a silicon microring resonator probed by stimulated four wave mixing," Sci. Rep. **6**, 23564 (2016).
15. W. Bogaerts, P. De Heyn, T. Van Vaerenbergh, K. De Vos, S. Kumar Selvaraja, T. Claes, P. Dumon, P. Bienstman, D. Van Thourhout, and R. Baets, "Silicon microring resonators," Laser Photon. Rev. **6**, 47–73 (2012).
16. Z. Vernon, M. Menotti, C. C. Tison, J. A. Steidle, M. L. Fanto, P. M. Thomas, S. F. Preble, A. M. Smith, P. M. Alsing, M. Liscidini, and J. E. Sipe, "Truly unentangled photon pairs without spectral filtering," Opt. Lett. **42**, 3638–3641 (2017).
17. S. Aaronson and A. Arkhipov, "The computational complexity of linear optics," in *43rd Annual ACM Symposium on Theory of Computing* (ACM, 2011), pp. 333–342.
18. A. Neville, C. Sparrow, R. Clifford, E. Johnston, P. M. Birchall, A. Montanaro, and A. Laing, "Classical boson sampling algorithms with superior performance to near-term experiments," Nat. Phys. **13**, 1153–1157 (2017).
19. A. Aspuru-Guzik and P. Walther, "Photonic quantum simulators," Nat. Phys. **8**, 285–291 (2012).
20. J. Huh, G. G. Guerreschi, B. Peropadre, J. R. McClean, and A. Aspuru-Guzik, "Boson sampling for molecular vibronic spectra," Nat. Photonics **9**, 615–620 (2015).
21. C. Sparrow, E. Martn López, N. Maraviglia, A. Neville, C. Harrold, J. Carolan, Y. N. Joglekar, T. Hashimoto, N. Matsuda, J. L. O'Brien, D. P. Tew, and A. Laing, "Simulating the vibrational quantum dynamics of molecules using photonics," Nature **557**, 660–667 (2018).
22. M. Gimeno-Segovia, P. Shadbolt, D. E. Browne, and T. Rudolph, "From three-photon Greenberger-Horne-Zeilinger states to ballistic universal quantum computation," Phys. Rev. Lett. **115**, 020502 (2015).

23. P. P. Rohde and T. C. Ralph, "Error tolerance of the boson-sampling model for linear optics quantum computing," Phys. Rev. A **85**, 022332 (2012).
24. V. S. Shchesnovich, "Sufficient condition for the mode mismatch of single photons for scalability of the boson-sampling computer," Phys. Rev. A **89**, 022333 (2014).
25. L. G. Helt, M. Liscidini, and J. E. Sipe, "How does it scale? Comparing quantum and classical nonlinear optical processes in integrated devices," J. Opt. Soc. Am. B **29**, 2199–2212 (2012).
26. R. S. Judson and H. Rabitz, "Teaching lasers to control molecules," Phys. Rev. Lett. **68**, 1500–1503 (1992).
27. H. Rabitz, R. de Vivie-Riedle, M. Motzkus, and K. Kompa, "Whither the future of controlling quantum phenomena?" Science **288**, 824–828 (2000).
28. C. Ferrie and O. Moussa, "Robust and efficient in situ quantum control," Phys. Rev. A **91**, 052306 (2015).
29. K. Padmaraju, D. F. Logan, T. Shiraishi, J. J. Ackert, A. P. Knights, and K. Bergman, "Wavelength locking and thermally stabilizing microring resonators using dithering signals," J. Lightwave Technol. **32**, 505–512 (2014).
30. F. Horst, W. M. J. Green, S. Assefa, S. M. Shank, Y. A. Vlasov, and B. J. Offrein, "Cascaded Mach-Zehnder wavelength filters in silicon photonics for low loss and flat pass-band WDM (de-) multiplexing," Opt. Express **21**, 11652–11657 (2013).
31. J. Michel, J. Liu, and L. C. Kimerling, "High-performance Ge-on-Si photodetectors," Nat. Photonics **4**, 527–534 (2010).
32. N. C. Harris, Y. Ma, J. Mower, T. Baehr-Jones, D. Englund, M. Hochberg, and C. Galland, "Efficient, compact and low loss thermo-optic phase shifter in silicon," Opt. Express **22**, 10487 (2014).
33. T. J. Seok, N. Quack, S. Han, R. S. Muller, and M. C. Wu, "Large-scale broadband digital silicon photonic switches with vertical adiabatic couplers," Optica **3**, 64–67 (2016).
34. D. J. Thomson, F. Y. Gardes, Y. Hu, G. Mashanovich, M. Fournier, P. Grosse, J.-M. Fedeli, and G. T. Reed, "High contrast 40Gbit/s optical modulation in silicon," Opt. Express **19**, 11507–11516 (2011).
35. B. E. Little, J.-P. Laine, and S. T. Chu, "Surface-roughness-induced contradirectional coupling in ring and disk resonators," Opt. Lett. **22**, 4–6 (1997).
36. J. A. Nelder and R. Mead, "A simplex method for function minimization," Comput. J. **7**, 308–313 (1965).
37. Z. Zhou, B. Yin, and J. Michel, "On-chip light sources for silicon photonics," Light Sci. Appl. **4**, e358 (2015).
38. M. Piekarek, D. Bonneau, S. Miki, T. Yamashita, M. Fujiwara, M. Sasaki, H. Terai, M. G. Tanner, C. M. Natarajan, R. H. Hadfield, J. L. O'Brien, and M. G. Thompson, "High-extinction ratio integrated photonic filters for silicon quantum photonics," Opt. Lett. **42**, 815–818 (2017).
39. Z. Wang, H. Liu, Q. Sun, N. Huang, S. Li, and J. Han, "The influence of thermal and free carrier dispersion effects on all-optical wavelength conversion in a silicon racetrack-shaped microring resonator," Laser Phys. **26**, 075403 (2016).
40. H. Lin, Z. Luo, T. Gu, L. C. Kimerling, K. Wada, A. Agarwal, and J. Hu, "Mid-infrared integrated photonics on silicon: a perspective," Nanophotonics **7**, 85 (2017).
41. Y. Zou, S. Chakravarty, C.-J. Chung, X. Xu, and R. T. Chen, "Mid-infrared silicon photonic waveguides and devices [Invited]," Photon. Res. **6**, 254–276 (2018).
42. A. H. Atabaki, S. Moazeni, F. Pavanello, H. Gevorgyan, J. Notaros, L. Alloatti, M. T. Wade, C. Sun, S. A. Kruger, H. Meng, K. Al Qubaisi, I. Wang, B. Zhang, A. Khilo, C. V. Baiocco, M. A. Popović, V. M. Stojanović, and R. J. Ram, "Integrating photonics with silicon nanoelectronics for the next generation of systems on a chip," Nature **556**, 349–354 (2018).
43. L. Carroll, J.-S. Lee, C. Scarcella, K. Gradkowski, M. Duperron, H. Lu, Y. Zhao, C. Eason, P. Morrissey, M. Rensing, S. Collins, H. Hwang, and P. O'Brien, "Photonic packaging: transforming silicon photonic integrated circuits into photonic devices," Appl. Sci. **6**, 426 (2016).
44. C. Schuck, W. H. P. Pernice, and H. X. Tang, "Waveguide integrated low noise NbTiN nanowire single-photon detectors with milli-Hz dark count rate," Sci. Rep. **3**, 1893 (2013).
45. E. Schelew, M. K. Akhlaghi, and J. F. Young, "Waveguide integrated superconducting single-photon detectors implemented as near-perfect absorbers of coherent radiation," Nat. Commun. **6**, 8233 (2015).
46. D. Zhu, Q.-Y. Zhao, H. Choi, T.-J. Lu, A. E. Dane, D. Englund, and K. K. Berggren, "A scalable multi-photon coincidence detector based on superconducting nanowires," Nat. Nanotechnol. **13**, 596–601 (2018).
47. M. Heuck, M. Pant, and D. R. Englund, "Temporally and spectrally multiplexed single photon source using quantum feedback control for scalable photonic quantum technologies," New J. Phys. **20**, 063046 (2018).
48. M. Pant, H. Krovi, D. Englund, and S. Guha, "Rate-distance tradeoff and resource costs for all-optical quantum repeaters," Phys. Rev. A **95**, 012304 (2017).